
TOWARDS EFFICIENT AND SECURE DELIVERY OF DATA FOR TRAINING AND INFERENCE WITH PRIVACY-PRESERVING

A PREPRINT

Juncheng Shen

College of Electrical Engineering
Zhejiang University
Hangzhou, Zhejiang, 310027, China
shenjc@zju.edu.cn

Juzheng Liu

Department of Physics
Tsinghua University
Beijing, 100084, China
liu-jz15@mails.tsinghua.edu.cn

Yiran Chen and Hai Li

Department of Electrical and Computer Engineering
Duke University
Durham, NC, 27708, USA
{yiran.chen, hai.li}@duke.edu

December 15, 2024

ABSTRACT

Privacy recently emerges as a severe concern in deep learning, e.g., sensitive data must be prohibited from being shared to the third party during deep neural network development. In this paper, we present *Morphed Learning* (MoLe), an efficient and secure scheme for delivering deep learning data. MoLe is consisted of data morphing and Augmented Convolutional (Aug-Conv) layer. Data morphing allows the data provider to send morphed data without privacy information, while Aug-Conv layer helps the deep learning developer apply their network on the morphed data without performance penalty. Theoretical analysis show that MoLe can provide strong security with overhead non-related to dataset size or the depth of neural network. Thanks to the low overhead, MoLe can be applied for both training and inference stages. Specifically, using MoLe for VGG-16 network on CIFAR dataset, the computational overhead is 9% and data transmission overhead is 5.12%. Meanwhile the attack success probability for the adversary is less than 7.9×10^{-90} .

1 Introduction

In recent years, deep learning has become the driving force for intelligent applications due to its rapid growth. With its success in image classification [1], object detection [2], speed recognition [3] and game intelligence [4], many has considered deep learning to be a viable path towards general artificial intelligence [5]. However, deep learning tends to have worse performance for real-world applications than in contained lab environments and a major reason is the lack of high quality training data for specific tasks [6]. Take medical imaging as an example, it is fundamentally a computer vision problem. Although deep learning usually prevails for computer vision tasks, the development of computational intelligent in this field still hardly meets expectations [7]. One of the main reasons is the difficulty of acquiring abundant data with regard to health and medical. These data contain sensitive and private information of individual patients, and therefore medical institutions are prohibited from sharing them due to legal and ethical concerns. The same struggle happens for all applications wherever privacy is involved, slowing down the adoption of deep learning.

The solution to this challenge boils down to securely separating the privacy information from data with minimum extra cost of computational resource and penalty to the performance of deep neural networks. Several implementations based on *Homomorphic Encryption* (HE) [8] or *Secure Multi-Party Computation* (SMC) [9] have been proposed. However, these attempts suffer from the limitation of their underlying cryptography techniques, introducing computational and data transmission overhead positively correlated to the depth of neural network. As the trend of deeper neural

networks [10, 11], depth correlated overhead would harm the practicality of these privacy-preserving schemes, especially for training. In addition to cryptography backed solutions, [12, 13] exploits property of the neural network itself, transmitting low-level extracted features instead of the original data. Though the feature transmitting methods can quarantine the original data, they compromise on network performance for security against reverse engineering attack.

In this paper, we propose *Morphed Learning* (MoLe), a privacy-preserving scheme for efficient and secure delivery of deep learning data which can be used both for training and inference stages. The main contributions of this paper are listed as follows:

1. We present *Data Morphing*, the first key component of MoLe. Data morphing serves as a linear shift in the multidimensional space for the original data. It blends each element in the data matrix with other elements, effectively hiding the sensitive information as the morphed data is unrecognizable by human observer.
2. We present *Augmented Convolutional* (Aug-Conv) layer, the other main component of MoLe. Aug-Conv layer is constructed as a combination of inverse transformation of data morphing and the first convolutional layer in the original neural network. By replacing the first convolutional layer, Aug-Conv layer can fully remedy the performance decrease of neural network training due to the spacial shift of inputs introduced by data morphing. The replacement is compatible to any convolutional neural network structures, adding no extra constrain to the network design.
3. We conduct security analysis in a theoretical way. Three possible attack schemes against MoLe are presented. The analysis show that the upper bound of adversary’s success probability is low even with a strict privacy reservation requirement. Specifically, the attack success probability for VGG-16 network on CIFAR is $P = 7.9 \times 10^{-90}$.
4. We conduct overhead analysis in a theoretical way. Both computational and transmission overhead are proven to be non-correlated to the depth of neural network or the size of the dataset, which makes MoLe applicable for complicated tasks. The low overhead of MoLe also ensures that it can be applied to both training and inference stages.
5. We use experiments to verify the effectiveness of Aug-Conv layer. Experiments on CIFAR-10 [14] show that replacing the first convolutional layer by Aug-Conv layer, the penalty of training performance for a VGG-16 network is within error margin.

The code to construct data morphing, Aug-Conv layer and to reproduce our experiments can be found in: https://github.com/NIPS2019-authors/MoLe_public

2 Preliminary

2.1 Terms and settings

In this subsection we introduce some terms and settings that apply for the rest of the paper. Imagine this situation, in which entity A owns a database of sensitive user information and entity B has a team of competent developers for deep learning applications. We use the term *data provider* to represent entity A and the term *developer* to refer to entity B. Sees the opportunity of creating value from big data using deep learning techniques, the data provider hopes to outsource the development task to the developer, and therefore he needs to transmit his data to the developer. To minimize the risk of potential user privacy leakage, the data provider requires a method to hide the private information within the data. On the other hand, the developer wishes the method to introduce no performance penalty and few structural constrain to his carefully-designed neural networks. For practicality concerns, both the data provider and the developer requires the overhead introduced by the method to be minimal.

The developer is considered to be a potential adversary, as he can profit from the private information in the data if he were able to recover them. In addition, for better real-world resemblance, we assume that the data provider only has the computational power equivalent to regular desktop PCs and therefore does not have adequate resource for large-scale neural network training. This is a reasonable assumption since neural network training is a computational intensive task and often requires dedicated hardware accelerators like high-end graphics cards [15].

2.2 Notations

In this subsection we introduce the notations system used in this paper. The notation follows two rules: 1. Bold font letters indicate matrices such as \mathbf{A} , and $A_{x,y}$ refers to the element with coordinate of (x, y) in \mathbf{A} . The element in the top-left corner is considered to be the origin. x axis indexes for rows and y axis indexes for columns. 2. $\mathbf{K}_{i,j}$ indicates a kernel for a convolutional layer, where i is the index for input channels and j is the index for output channels. Combining the two rules, $k_{(i,j),(x,y)}$ stands for the element with coordinate (x, y) in $\mathbf{K}_{i,j}$. All the coordinates of matrices in this paper use zero based indexing.

2.3 Related work

To provide computational service for unobservable data has long been considered as the holy grail for cryptographers, as it offers a higher level of security and lowers the cost of trust. We categorize the cryptography based data delivery schemes for deep learning depending on whether they are built on HE or SMC [16]. Other non cryptography based solutions are detailed as well.

HE based data delivery for deep learning. The idea of HE is to compute on ciphertext and generate the ciphertext of result which can be decrypted to original result. However, due to its computational expensive nature, approaches based on HE [17, 18, 19] only focused on the inference stage of deep learning, leaving the privacy information in training dataset unprotected. Even only for inference, HE based solutions tend to have high computational cost, as the latest work [19] reported that running encrypted MNIST dataset on a 16-core workstation took 2 hours, while running plain MNIST dataset on a regular PC takes a few minutes. HE based schemes also constrains the design of neural network, as both [18] and [19] restricts the range of activation to be discretized or even binarized.

SMC based data delivery for deep learning. In SMC, multiple parties hold their own private data, and they wish to jointly compute a function that is dependent to data of all parties without each party acquiring the data of other parties. Following the idea of SMC, distributed selective SGD was proposed [20], featuring a centralized parameter server for gradient transferring. However, recent study [21] discovered a security flaw in [20] as the parameter server is capable of recover training data with gradients. In addition, approaches combining HE and a subfield of SMC, namely two-party computation (2PC), were proposed to provide privacy-preserving for both training and inference stages [22, 23, 24]. However the computational overhead for this kind of solutions is still not ideal, as the latest work [24] reported 421,000 times of data transmission overhead and more than 10,000 times of execution time overhead, compared to non privacy-preserving method.

Feature transmission based data delivery for deep learning. Unlike cryptography based schemes, feature transmission based schemes [12, 13] utilize the property of neural network itself. Instead of sending the original data, the data provider computes several layers of the neural network and then send the extracted features, which reduces the practicality as he may lack the computational power for neural network computing. Furthermore, features usually have more channels than the original data which would increase the data transmission. To combat reverse engineering, noise is applied to the features and thus results in the degradation of network performance. [13] reported 62.8% of higher error rate for CIFAR-10 dataset.

Differential privacy. Differential privacy is a popular technique of privacy-preserving for deep learning applications, which is usually used for one of the two goals: 1. Preventing adversary from identifying or recovering training data from a published network model [25]; 2. To enhance security for collaborative training schemes against reverse engineering on shared gradients [26]. The first usage is for the defense of inversion attacks and thus it is not in the scope of this paper. The second usage suffers a fatal security vulnerability, as malicious participant can breach the differential privacy by prototypical data generated by GANs [27]. For these two reasons, we do not compare our work with differential privacy based privacy-preserving schemes.

3 Method

MoLe consists of two main components which are named as data morphing and Aug-Conv layer respectively. Data morphing serves for the data provider, as it provides human unrecognizable data transformation and can be efficiently computed by consumer-level CPUs. Aug-Conv layer fully compensates the performance decrease of neural network due to data morphing, and it is compatibility for all convolutional neural network structures. Figure 1 describes the process of utilizing MoLe for privacy-preserving. First, the developer trains his network on a public dataset similar to the dataset of data provider’s, and sends the first trained convolutional layer to the data provider. Then, the data provider generates the morphing matrix and Aug-Conv layer, and uses data morphing to transform his data; The developer replaces the first convolutional layer in his network, and then conducts training and inference on morphed data without the need of modifying the rest part of his design. During the training process, developer treats the Aug-Conv layer as a fixed feature extractor similarly to pre-trained layers in transfer learning [28, 29]. In this section and section 4, we assume the attributions of the first convolution layer to be: the shape of input data is $m \times m$ with α channels, the shape of output features is $n \times n$ with β channels and the shape of convolutional kernel is $p \times p$.

3.1 Data to row vector

Converting the first convolutional layer to an equivalent matrix multiplication is the foundation for both data morphing and Aug-Conv layer. Image to column matrix (im2col) is a trick to increase data parallelism for convolutional layer, and it has been widely implemented in varies of deep learning frameworks [15, 30, 31]. The goal of im2col is to convert

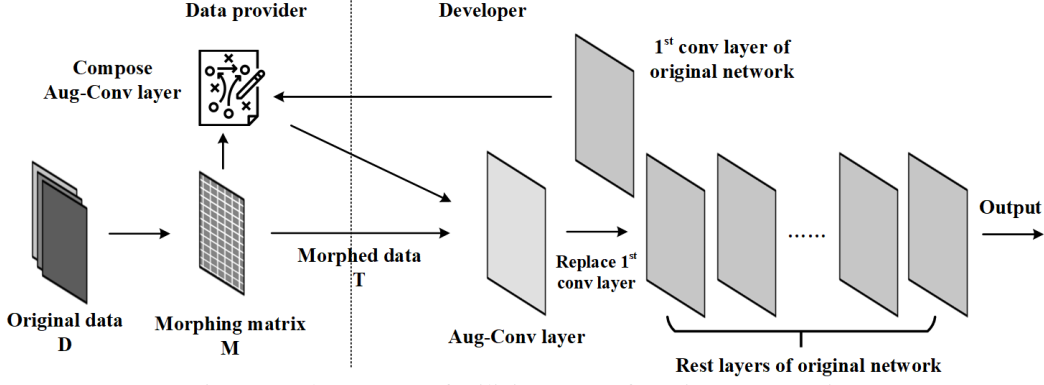


Figure 1: The process of utilizing MoLe for privacy-preserving.

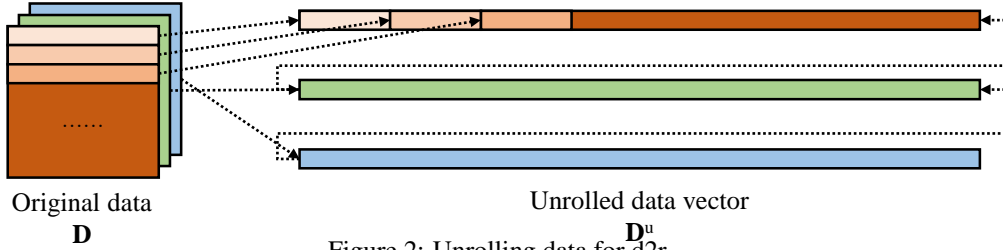


Figure 2: Unrolling data for d2r.

convolutional layer from sliding convolutional kernels on the input data to matrix-matrix multiplication [32]. On the other hand, d2r is a more extreme version of im2col, converting the convolutional layer to the product of a row vector and a large matrix. The detailed steps of d2r are:

1. Unroll the input data \mathbf{D} to row vectors. First unroll the data of each channel by placing the row vector with smaller row index at left, and then concatenate each channel vector by placing the channel with smaller channel index at left. The unrolled data vector \mathbf{D}^r has the shape of $1 \times \alpha m^2$. The unrolling process is depicted in figure 2.
2. Replace the convolution operation to a large matrix \mathbf{C} whose shape is $\alpha m^2 \times \beta n^2$. First initialize \mathbf{C} with zero elements. Then, for every weight $k_{(i,j),(a,b)}$, assign $C_{x,y} = k_{(i,j),(a,b)}$ when (x,y) satisfies equation 1:

$$\begin{aligned} x &= im^2 + am + cm + b + d \\ y &= jn^2 + cn + d \end{aligned} \quad (1)$$

where $i \in [0, \alpha)$ is the index for input channels; $j \in [0, \beta)$ is the index for output channels; (c, d) is the coordinate for input data and $c, d \in [0, m - p + 1)$; $a, b \in [0, p)$ are the coordinate for kernels.

3. After multiplying \mathbf{D}^r and \mathbf{C} , we can get a row vector \mathbf{F}^r with the shape of $1 \times \beta n^2$. Following the same rules in step 1 reversely, the features identical to the output of original convolutional operation can be reconstructed.

Figure 3 shows the process of using d2r to compute convolutional layer operation. In the rest of the paper, matrix with superscript r represents its d2r unrolled row vector.

3.2 Data morphing

Data morphing is designed to meet the following three requirements. 1. *Equal-sized input and output data*: This requirement ensures that the data transmission overhead does not have a correlation to the amount of data; 2. *Adjustable computation cost*: This requirement comes from the setting in section 2.1, as the data provider may have limited computational power; 3. *Unrecognizable transformation*: Data morphing should provide unrecognizable result to human observers for privacy-preserving purpose.

Before data morphing, the original data \mathbf{D} is unrolled to \mathbf{D}^r using d2r. The data morphing operation can be described by equation 2:

$$\mathbf{D}^r \cdot \mathbf{M} = \mathbf{T}^r \quad (2)$$

where \mathbf{T}^r is a row vector representing the morphed data. \mathbf{M} is the morphing matrix, which is composed as follows:

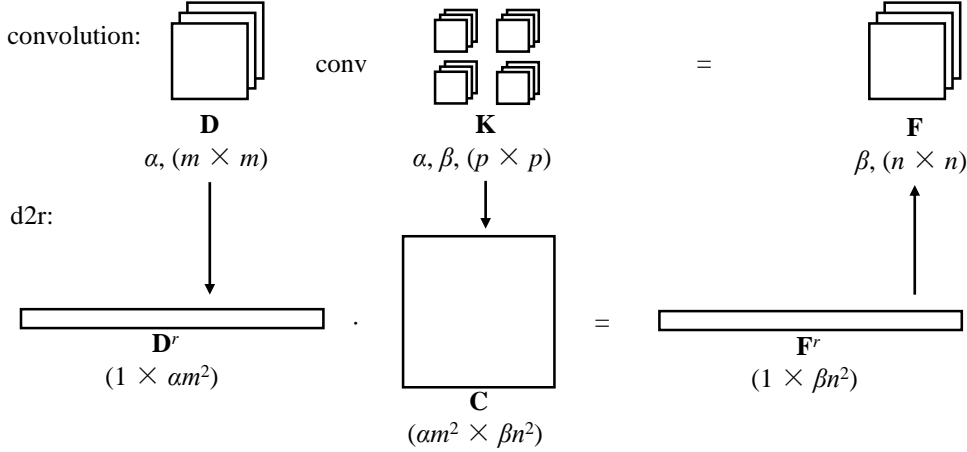
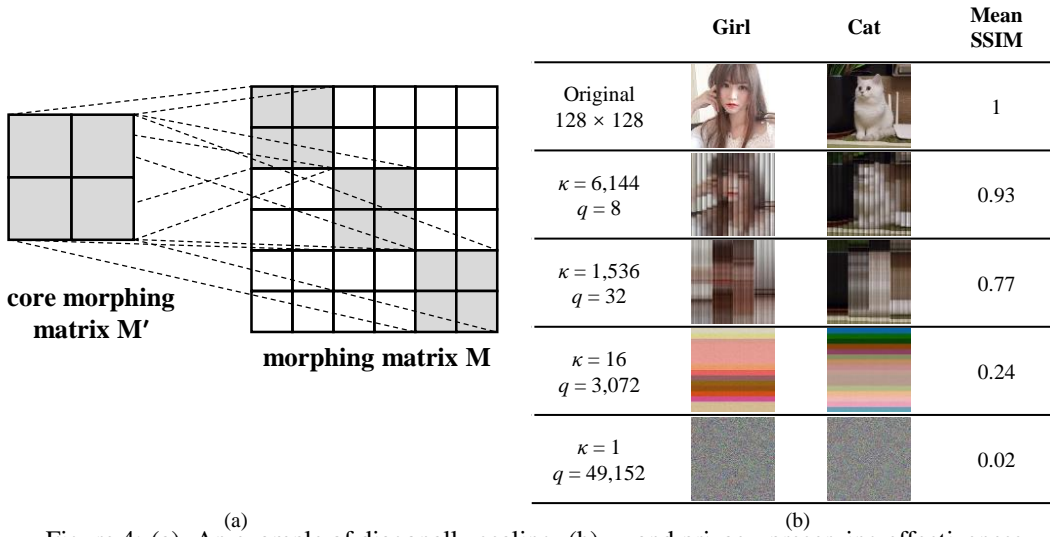


Figure 3: Using d2r to compute convolutional layer.

Figure 4: (a). An example of diagonally scaling. (b). κ and privacy-preserving effectiveness.

1. Compose core morphing matrix \mathbf{M}' . \mathbf{M}' is a reversible matrix, and all of its elements are random and non-zero. Assume the shape of \mathbf{M}' is $q \times q$, q should satisfy equation 3:

$$\kappa = \frac{\alpha m^2}{q} \in \mathbb{Z}^+ \quad (3)$$

Here κ is called the morphing scale factor.

2. Compose \mathbf{M} by diagonally scaling \mathbf{M}' to $\alpha m^2 \times \alpha m^2$. The correlation between the two matrices can be written as equation 4:

$$M_{x,y} = \begin{cases} M'_{x-Nq, y-Nq}, & x \in [Nq, (N+1)q) \wedge y \in [Nq, (N+1)q) \\ 0, & \text{else} \end{cases} \quad (4)$$

where N satisfies $N \in \mathbb{N} \wedge N < \kappa$.

Figure 4(a) shows an example of diagonally scaling \mathbf{M}' with the shape of 2×2 to compose \mathbf{M} with the shape of 6×6 . The computational cost of data morphing increases as κ decreases, since there are fewer zero elements with larger p .

The morphing scaling factor κ controls the trade-off between the computational cost and the effectiveness of privacy-preserving. This is shown in figure 4(b) using two real-world photos. Structural similarity (SSIM) index [33] in the figure is a commonly used method to evaluate the visual similarity between two images. SSIM index ranges from 0 to 1, and larger value means higher visual similarity. We use SSIM index to assess the effectiveness of privacy-preserving, as lower SSIM index between \mathbf{T} and \mathbf{D} means the privacy information in the original data is more unrecognizable. Since recent study [34] showed that modern desktop CPUs with support of AVX instructions can compute simple matrix multiplications with decent efficiency, it is recommended to use a larger morphing core for better privacy when data

provider has the computational power equivalent to desktop PCs. However, for lower end compute devices such as embedded systems, data morphing does provide less computational hungry operation at the cost of privacy.

It is worth noting that the privacy-preserving feature provided by data morphing relies on the secure storage of \mathbf{M} , similarly to how the security of symmetric key encryption relies on the secure storage of secret keys. Once the developer were able to acquire \mathbf{M} , he could recover the original data by $\mathbf{D}^r = \mathbf{T}^r \cdot \mathbf{M}^{-1}$, where \mathbf{M}^{-1} is the inverse matrix of \mathbf{M} .

3.3 Augmented convolutional layer

The design of Aug-Conv layer complies with the three requirements. 1. *Equivalent feature extraction for morphed data*: It ensures that the developer can train his network to achievement same performance on morphed data without modifying the design of network; 2. *Resistance to reverse engineering attack*: The Aug-Conv layer should not reveal the detail of the morphing matrix \mathbf{M} under reverse engineering attack. 3. *Resistance to reverse convolutional operation attack*: Though the Aug-Conv layer needs to extract equivalent features, it should not provide identical features or otherwise the developer could recover the original data using the reverse operation of convolutional layer.

Inverse matrix combination. After d2r, the convolutional operation for the original first layer is converted into \mathbf{C} with the shape of $\alpha m^2 \times \beta n^2$, which enables the combination of \mathbf{M}^{-1} and \mathbf{C} to form the Aug-Conv layer. The steps of inverse matrix combination are:

1. Calculate inverse morphing matrix \mathbf{M}^{-1} . When using d2r for convolutional operation, \mathbf{M}^{-1} can restore the row vector of morphed data \mathbf{T}^r back to \mathbf{D}^r , which can be represented as $\mathbf{T}^r \cdot \mathbf{M}^{-1} = \mathbf{D}^r$.
2. Combining \mathbf{M}^{-1} and \mathbf{C} to form the Aug-Conv layer \mathbf{C}^{ac} by $\mathbf{C}^{ac} = \mathbf{M}^{-1} \cdot \mathbf{C}$.

At this point, the features extracted by Aug-Conv layer from morphed data is identical to the features extracted by the convolutional layer from original data, as illustrated in equation 5:

$$\mathbf{T}^r \cdot \mathbf{C}^{ac} = \mathbf{T}^r \cdot \mathbf{M}^{-1} \cdot \mathbf{C} = \mathbf{D}^r \cdot \mathbf{C} = \mathbf{F}^r \quad (5)$$

Although \mathbf{C} is trained on another similar dataset, it can still be used for \mathbf{D} , since low-level feature extractor for similar tasks show strong transferability [29], and therefore the first requirement of Aug-Conv layer is met. The combination also serves for the second requirement, as it blends the inverse matrix \mathbf{M}^{-1} with the convolutional matrix.

Feature channel randomization. The \mathbf{C}^{ac} composed only with inverse matrix combination suffers the vulnerability of reserve convolutional operation attack. As shown in figure 1, \mathbf{C} is provided by the developer, and thus he can also acquire its reverse operation \mathbf{C}^{-1} . As a result, the developer can recover the original data by: $\mathbf{D}^r = \mathbf{F}^r \cdot \mathbf{C}^{-1}$. For the third requirement of Aug-Conv layer, we randomly shuffle the channels of output features to combat this threat. Assume $\mathbf{F}' = rand(\mathbf{F})$ is the output features with randomized channel order and *rand* is the randomization function, \mathbf{F}' and \mathbf{F} are two sets of equivalent features for the rest layers of the neural network, as the shuffled channel order can be learned by the rest layers in training. On the other hand, function *rand* prevents the developer from restoring the original data as $\mathbf{D}^r \neq rand(\mathbf{F}^r) \cdot \mathbf{C}^{-1}$ and therefore the third requirement is met. Similarly to \mathbf{M} , the detailed channel order used for *rand* needs to be stored securely.

The following two steps enhance \mathbf{C}^{ac} by implementing *rand* function into the matrix: 1. Separate \mathbf{C}^{ac} into β groups and each group contains n^2 continuous columns. 2. Randomly shuffle the order of the column groups to construct the new Aug-Conv layer matrix.

4 Analysis

4.1 Threat model

The developer is considered to be an *Honest-but-Curious* (HBC) adversary. HBC is a typical threat model for SMC, in which the adversary tries to discover as much information from other parties as possible without violating the protocol. The HBC setting for MoLe means that the developer tries to recover original data using the information sent from the data provider, including \mathbf{T} and \mathbf{C}^{ac} . The developer does not exploit other security breaches to get access of \mathbf{M}^{-1} , *rand* or \mathbf{D} .

Additionally, *Semi-Honest-but-Curious* (SHBC) adversarial model is another stronger threat model, in which the developer is capable of acquiring several \mathbf{D} - \mathbf{T} pairs. The SHBC model allows further analysis for the situations where the adversary managed to inject some of his own data into the data provider's database beforehand.

4.2 Security analysis

In this subsection, the security of MoLe against three possible attack methods is quantitatively analyzed in the form of attack success probability. The three attack methods are *Brute Force Attack*, *Aug-Conv Reversing Attack* and *D-T Pair Attack*.

Definition 1. Unit l^2 -norm matrix. Any matrix \mathbf{A} that satisfies $|\mathbf{A}|_2 = 1$ is a unit l^2 -norm matrix, where $|\mathbf{A}|_2$ denotes the l^2 -norm for \mathbf{A} .

For a clear elaboration, in this section we assume \mathbf{D}^r and each column in \mathbf{M} are all unit l^2 matrices.

Brute Force Attack. The most straightforward attack to MoLe in HBC setting is to apply brute force attack on \mathbf{M} . Suppose the attack matrix is \mathbf{G} . Unlike encryption keys which would be useless even with one-bit difference, a close approximation of \mathbf{M} can also recover recognizable data \mathcal{D}^r as shown in equation 6:

$$\mathbf{G} \approx \mathbf{M} \Rightarrow \mathbf{G}^{-1} \approx \mathbf{M}^{-1} \Rightarrow \mathcal{D}^r = \mathbf{T}^r \cdot \mathbf{G}^{-1} \approx \mathbf{T}^r \cdot \mathbf{M}^{-1} = \mathcal{D}^r \quad (6)$$

Lemma 1. Assume \mathbf{A} is a given unit l^2 -norm matrix which has N elements, P_1 is the probability of a random unit l^2 -norm \mathbf{B} that satisfies equation 7:

$$|\mathbf{A} - \mathbf{B}|_2 \leq d \leq 1 \quad (7)$$

The upper bound for P_1 can be represented as equation 8:

$$P_1 \leq \frac{1}{2}d^{(N-1)} \quad (8)$$

Lemma 2. Assume $E_{sd}(\mathbf{D}^r, \mathcal{D}^r)$ is the standard deviation between \mathbf{D}^r and \mathcal{D}^r , N is the number of elements in morphing core \mathbf{M}' , P_2 is the probability of $E_{sd}(\mathbf{D}^r, \mathcal{D}^r) \leq \sigma$. P_2 satisfies equation:

$$P_2 = P_1(d = \sigma) \quad (9)$$

where P_1 is the probability in lemma 1.

Substitute lemma 1 into lemma 2*, we can prove theorem 1:

Theorem 1. For original data \mathbf{D}^r and recovered data \mathcal{D}^r , \mathbf{M}' has $N = (\frac{\alpha m^2}{\kappa})^2$ elements, the probability $P_{M,bf}$ for $E_{sd}(\mathbf{D}^r, \mathcal{D}^r) \leq \sigma$ has the upper bound of:

$$P_{M,bf} \leq \frac{1}{2}\sigma^{N-1} = \frac{1}{2}\sigma^{(\frac{\alpha m^2}{\kappa})^2-1} \quad (10)$$

$E_{sd}(\mathbf{D}^r, \mathcal{D}^r)$ is considered to be the privacy reservation R_p for MoLe, directing the maximum resemblance between \mathbf{D}^r and \mathcal{D}^r allowed by the data provider. $R_p \in (0, 1)$ and larger R_p means stricter requirement for privacy-preserving.

The adversary can also apply brute force attack on *rand*. There are $\beta!$ possible randomization orders and therefore the success probability for brute force attack on *rand* is $P_{r,bf} = \frac{1}{\beta!}$.

To provide an intuitive understanding for the probabilities, we take CIFAR dataset as an example. Assume the data provider requires $R_p = 50\%$ [†] chooses $\kappa = 1$, the network used by the data provider is VGG-16[35]. In this setting, $N = \frac{\alpha^2 m^4}{\kappa^2} = 3072^2$ and we can get $P_{M,bf} \leq 2^{-3072^2} \approx 2^{-9 \times 10^6}$, and $P_{r,bf} = (64!)^{-1} \approx 7.9 \times 10^{-90}$.

Aug-Conv Reversing Attack. Aug-Conv reversing attack is another viable method for HBC setting, in which the adversary tries to factorize \mathbf{C}^{ac} to acquire \mathbf{M}^{-1} and *rand*(\mathbf{C}). Consider the channel with index of j in the output features, the factorization process is to solve the equation set 11:

$$\mathbf{C}_y^{ac} = \mathbf{M}^{-1} \cdot \mathbf{C}_y \quad (11)$$

where \mathbf{C}_y^{ac} and \mathbf{C}_y each means the column vector with the index of y in \mathbf{C}^{ac} and \mathbf{C} respectively, $y \in [jn^2, (j+1)n^2)$.

In equation set 11, \mathbf{M}^{-1} is unknown to the adversary, introducing $\frac{\alpha m^2}{\kappa}$ unknown vector variables. In HBC settings, the adversary does not have access to *rand* and therefore *rand*(\mathbf{C}) is also unknown, introducing $\alpha\beta p^2$ unknown elemental variables. The total number of unknown variables for the adversary is:

$$N_{unk} = \frac{\alpha m^2}{\kappa} + \alpha p^2 > \frac{\alpha m^2}{\kappa} \quad (12)$$

*The proof for lemma 1 and 2 can be found in supplementary material.

[†] $R_p = 50\%$ is already a very strict privacy-preserving requirement. A pair of \mathbf{D}^r and \mathcal{D}^r with $R_p = 50\%$ can be found in supplementary material.

The number of equations in equation set 11 is $N_{eq} = n^2$. To prevent the adversary from solving the equation set, N_{unk} should be larger than N_{eq} , and therefore κ should satisfy:

$$\frac{\alpha m^2}{\kappa} \geq n^2 \Rightarrow \kappa \leq \frac{\alpha m^2}{n^2} \quad (13)$$

Here we manage to determine the upper bound for κ . Additionally, even if the adversary includes more input channels into the equation set, each channel can only provide αp^2 independent equations while also introducing another αp^2 unknown variables. Thus including more input channels does not help the adversary to solve the equation set.

The adversary can use equation set 11 to represent N_{eq} elements in a column vector of \mathbf{M}^{-1} with other elements. By eliminating n^2 independent elements in each column, the adversary can have a higher success probability $P_{M,ar}$ which can be represented as equation 14:

$$P_{M,ar} = P_{M,bf} \left(N = \left(\frac{\alpha m^2}{\kappa} - n^2 \right) \left(\frac{\alpha m^2}{\kappa} \right) + \alpha p^2 \right) \leq \frac{1}{2} \sigma^{\left(\frac{\alpha m^2}{\kappa} - n^2 \right) \left(\frac{\alpha m^2}{\kappa} \right) + \alpha p^2 - 1} \quad (14)$$

With the same CIFAR dataset and VGG-16 network setting for brute force attack, We can get $P_{M,ar} \leq 2^{-3072 \times 2048} \approx 2^{-6 \times 10^6}$. For more complicated tasks like ImageNet [36], we can expect even higher level of security as both m and n increase.

D-T Pair Attack. D-T pair attack applies only to the SHBC threat model. For this attack, we use the number of \mathbf{D}^r - \mathbf{T}^r pairs required by the adversary to evaluate the security. In D-T pair attack, the adversary aims to calculate \mathbf{M}' by equation 15:

$$\mathbf{M}' = \mathbb{D}^{-1} \cdot \mathbb{T} \quad (15)$$

where \mathbb{D} and \mathbb{T} are constructed by stacking multiple \mathbf{D}^r - \mathbf{T}^r pairs correspondingly. We can see from equation 15 that the required number of D-T pair equals to the number of rows in \mathbf{M}' , which is $q = \frac{\alpha m^2}{\kappa}$. For the same setting in brute force attack, the attack requires 3,072 \mathbf{D}^r - \mathbf{T}^r pairs.

4.3 Overhead analysis

Computational overhead. The computational overhead introduced by MoLe are divided into two parts. The first part is on the data provider's end, caused by the calculation of equation 2. The second part is on the developer's end, due to replacing \mathbf{C} with \mathbf{C}^{ac} . We use the number of extra *Multiply-Accumulate* (MAC) operations to measure the computational overhead. For the data provider, for each calculation of equation 2, the total number of MAC operations $O_{comp,dp}$ can be represented as equation 16:

$$O_{comp,dp} = \alpha q^2 \quad (16)$$

in which multiplication with zero element is omitted. For the developer, the computational overhead $O_{comp,dev}$ is the difference between the MAC operations need by calculating $\mathbf{T}^r \cdot \mathbf{C}^{ac}$ and $\mathbf{D}^r \cdot \mathbf{C}$, which can be represented as equation 17:

$$O_{comp,dev} = \alpha m^2 \beta n^2 - \alpha p^2 \beta n^2 = (m^2 - p^2) \alpha \beta n^2 \quad (17)$$

We can see from equation 16 and 17 that either $O_{comp,dp}$ nor $O_{comp,dev}$ is related to the depth of the neural network.

On the other hand, we can also see that the computational overhead grows squarely to the size of input data m and output feature n , making MoLe more suitable for low dimensional tasks. To put it in perspective, the computational overhead proportion to the original network is 9% for VGG-16 network on CIFAR dataset, and 10 times for ResNet-152 network on ImageNet dataset.

Data transmission overhead. Since \mathbf{D}^r and \mathbf{T}^r has the same shape, the data transmission overhead O_{data} is solely for transmitting \mathbf{C}^{ac} . $O_{data} = (\alpha m^2)^2$ equals to the number of elements in \mathbf{C}^{ac} . O_{data} is irrelevant to either the number of data in the dataset or the depth of the neural network. For CIFAR dataset, O_{data} is 5.12% to the whole dataset, and the percentage drops as the size of dataset increases. For larger datasets like ImageNet, O_{data} is merely 1%.

4.4 Experimental analysis

Although we have proven that with the help of \mathbf{C}^{ac} , using MoLe for privacy-preserving does not hurt the neural network's performance, it is still theoretically harder to train a network with \mathbf{C}^{ac} as the network has to learn the feature randomization additionally. Therefore we use experiments on CIFAR dataset to verify the effectiveness of Aug-Conv layer. We trained three group of networks and the results are: 1. VGG-16 on original CIFAR-10 and CIFAR-100 dataset achieved 87.2% and 55.9% test accuracy respectively; 2. VGG-16 with its first layer replaced by Aug-Conv layer on morphed CIFAR-10 and CIFAR-100 dataset achieved 87.4% and 56.4% test accuracy respectively, and we

consider the performance difference between the first two groups is within error margin; 3. For sanity check, VGG-16 without Aug-Conv layer on morphed CIFAR-10 and CIFAR-100 dataset achieved 15.8% and 2.01% test accuracy respectively. The result shows that Aug-Conv layer can help network to archive its expected performance on morphed data. Contrarily, without the help of Aug-Conv layer, network performance would drop significantly.

At last, table 1 compares the performance penalty and overhead of MoLe with other related methods with the VGG-16 network and CIFAR dataset setting.

Table 1: The comparison between MoLe and other related methods.

Method	Performance penalty	Data transmission overhead	Computational overhead
MoLe	0	$0.05\times$	$0.09\times$
SMC based[24]	0	$421,000\times$	$10,000\times$
Feature transmission based[13]	$0.628\times$ higher error rate	$64\times$	0

References

- [1] Kaiming He, Xiangyu Zhang, Shaoqing Ren, and Jian Sun. Deep residual learning for image recognition. In *Proceedings of the IEEE Conference on Computer Vision and Pattern Recognition (CVPR)*, pages 770–778, 2016.
- [2] Kaiming He, Georgia Gkioxari, Piotr Dollár, and Ross Girshick. Mask r-cnn. In *Proceedings of the IEEE International Conference on Computer Vision (ICCV)*, pages 2961–2969, 2017.
- [3] Yanzhang He, Tara N Sainath, Rohit Prabhavalkar, Ian McGraw, Raziell Alvarez, Ding Zhao, David Rybach, Anjuli Kannan, Yonghui Wu, Ruoming Pang, et al. Streaming end-to-end speech recognition for mobile devices. In *Proceedings of the IEEE International Conference on Acoustics, Speech and Signal Processing*, pages 6381–6385, 2019.
- [4] David Silver, Thomas Hubert, Julian Schrittwieser, Ioannis Antonoglou, Matthew Lai, Arthur Guez, Marc Lanctot, Laurent Sifre, Dhharshan Kumaran, Thore Graepel, et al. A general reinforcement learning algorithm that masters chess, shogi, and go through self-play. *Science*, 362(6419):1140–1144, 2018.
- [5] Li Deng. Artificial intelligence in the rising wave of deep learning: The historical path and future outlook [perspectives]. *IEEE Signal Processing Magazine*, 35(1):180–177, 2018.
- [6] Gary Marcus. Deep learning: A critical appraisal. *arXiv preprint arXiv:1801.00631*, 2018.
- [7] Eliza Strickland. How IBM Watson overpromised and underdelivered on AI health care. <https://spectrum.ieee.org/biomedical/diagnostics/how-ibm-watson-overpromised-and-underdelivered-on-ai-health-care>, 2019.
- [8] Craig Gentry and Dan Boneh. *A fully homomorphic encryption scheme*. Stanford University, Stanford, 2009.
- [9] Andrew Chi-Chih Yao. Protocols for secure computations. In *Annual Symposium on Foundations of Computer Science (FOCS)*, volume 82, pages 160–164, 1982.
- [10] Yihui He, Xiangyu Zhang, and Jian Sun. Channel pruning for accelerating very deep neural networks. In *Proceedings of the IEEE International Conference on Computer Vision (ICCV)*, pages 1389–1397, 2017.
- [11] Tom Sercu, Christian Puhresch, Brian Kingsbury, and Yann LeCun. Very deep multilingual convolutional neural networks for lvsr. In *Proceedings of the International Conference on Acoustics, Speech and Signal Processing (ICASSP)*, pages 4955–4959, 2016.
- [12] Seyed Ali Osia, Ali Shahin Shamsabadi, Ali Taheri, Kleomenis Katevas, Sina Sajadmanesh, Hamid R Rabiee, Nicholas D Lane, and Hamed Haddadi. A hybrid deep learning architecture for privacy-preserving mobile analytics. *arXiv preprint arXiv:1703.02952*, 2017.
- [13] Ji Wang, Jianguo Zhang, Weidong Bao, Xiaomin Zhu, Bokai Cao, and Philip S Yu. Not just privacy: Improving performance of private deep learning in mobile cloud. In *Proceedings of the ACM SIGKDD International Conference on Knowledge Discovery & Data Mining (KDD)*, pages 2407–2416, 2018.
- [14] Alex Krizhevsky and Geoffrey Hinton. *Learning multiple layers of features from tiny images*. University of Toronto, Toronto, 2009.
- [15] Yangqing Jia, Evan Shelhamer, Jeff Donahue, Sergey Karayev, Jonathan Long, Ross Girshick, Sergio Guadarrama, and Trevor Darrell. Caffe: Convolutional architecture for fast feature embedding. In *Proceedings of the ACM International Conference on Multimedia*, pages 675–678, 2014.
- [16] Ho Bae, Jaehee Jang, Dahuin Jung, Hyemi Jang, Heonseok Ha, and Sungroh Yoon. Security and privacy issues in deep learning. *arXiv preprint arXiv:1807.11655*, 2018.
- [17] Ran Gilad-Bachrach, Nathan Dowlin, Kim Laine, Kristin Lauter, Michael Naehrig, and John Wernsing. Cryptonets: Applying neural networks to encrypted data with high throughput and accuracy. In *International Conference on Machine Learning (ICML)*, pages 201–210, 2016.
- [18] Florian Bourse, Michele Minelli, Matthias Minihold, and Pascal Paillier. Fast homomorphic evaluation of deep discretized neural networks. In *Annual International Cryptology Conference*, pages 483–512. Springer, 2018.
- [19] Amartya Sanyal, Matt Kusner, Adria Gascon, and Varun Kanade. Tapas: Tricks to accelerate (encrypted) prediction as a service. In *International Conference on Machine Learning (ICML)*, pages 4497–4506, 2018.
- [20] Reza Shokri and Vitaly Shmatikov. Privacy-preserving deep learning. In *Proceedings of the ACM SIGSAC Conference on Computer and Communications Security*, pages 1310–1321, 2015.
- [21] Yoshinori Aono, Takuya Hayashi, Lihua Wang, Shiho Moriai, et al. Privacy-preserving deep learning via additively homomorphic encryption. *IEEE Transactions on Information Forensics and Security*, 13(5):1333–1345, 2018.

- [22] Jian Liu, Mika Juuti, Yao Lu, and N Asokan. Oblivious neural network predictions via MiniONN transformations. In *Proceedings of ACM SIGSAC Conference on Computer and Communications Security*, pages 619–631. ACM, 2017.
- [23] Bitar Darvish Rouhani, M Sadegh Riazi, and Farinaz Koushanfar. Deepsecure: Scalable provably-secure deep learning. In *Proceedings of the Annual Design Automation Conference (DAC)*, page 2, 2018.
- [24] Chiraag Juvekar, Vinod Vaikuntanathan, and Anantha Chandrakasan. GAZELLE: A low latency framework for secure neural network inference. In *USENIX Security Symposium*, pages 1651–1669, 2018.
- [25] NhatHai Phan, Yue Wang, Xintao Wu, and Dejing Dou. Differential privacy preservation for deep auto-encoders: an application of human behavior prediction. In *AAAI Conference on Artificial Intelligence*, 2016.
- [26] Martin Abadi, Andy Chu, Ian Goodfellow, H Brendan McMahan, Ilya Mironov, Kunal Talwar, and Li Zhang. Deep learning with differential privacy. In *Proceedings of the ACM SIGSAC Conference on Computer and Communications Security*, pages 308–318, 2016.
- [27] Briland Hitaj, Giuseppe Ateniese, and Fernando Pérez-Cruz. Deep models under the GAN: Information leakage from collaborative deep learning. In *Proceedings of the ACM SIGSAC Conference on Computer and Communications Security*, pages 603–618, 2017.
- [28] Ali Sharif Razavian, Hossein Azizpour, Josephine Sullivan, and Stefan Carlsson. Cnn features off-the-shelf: an astounding baseline for recognition. In *Proceedings of the IEEE Conference on Computer Vision and Pattern Recognition Workshops (CVPR-W)*, pages 806–813, 2014.
- [29] Jason Yosinski, Jeff Clune, Yoshua Bengio, and Hod Lipson. How transferable are features in deep neural networks? In *Advances in Neural Information Processing Systems (NIPS)*, pages 3320–3328, 2014.
- [30] Martín Abadi, Paul Barham, Jianmin Chen, Zhifeng Chen, Andy Davis, Jeffrey Dean, Matthieu Devin, Sanjay Ghemawat, Geoffrey Irving, Michael Isard, et al. Tensorflow: A system for large-scale machine learning. In *USENIX Symposium on Operating Systems Design and Implementation (OSDI)*, pages 265–283, 2016.
- [31] Adam Paszke, Sam Gross, Soumith Chintala, Gregory Chanan, Edward Yang, Zachary DeVito, Zeming Lin, Alban Desmaison, Luca Antiga, and Adam Lerer. Automatic differentiation in PyTorch. In *NIPS 2017 Autodiff Workshop*, 2017.
- [32] Kumar Chellapilla, Sidd Puri, and Patrice Simard. High performance convolutional neural networks for document processing. In *International Workshop on Frontiers in Handwriting Recognition*, 2006.
- [33] Zhou Wang, Alan C Bovik, Hamid R Sheikh, Eero P Simoncelli, et al. Image quality assessment: From error visibility to structural similarity. *IEEE Transactions on Image Processing*, 13(4):600–612, 2004.
- [34] Somaia Awad Hassan, AM Hemeida, and Mountasser MM Mahmoud. Performance evaluation of matrix-matrix multiplications using intel’s advanced vector extensions (AVX). *Microprocessors and Microsystems*, 47:369–374, 2016.
- [35] Karen Simonyan and Andrew Zisserman. Very deep convolutional networks for large-scale image recognition. *arXiv preprint arXiv:1409.1556*, 2014.
- [36] Jia Deng, Wei Dong, Richard Socher, Li-Jia Li, Kai Li, and Li Fei-Fei. Imagenet: A large-scale hierarchical image database. In *IEEE Conference on Computer Vision and Pattern Recognition (CVPR)*, pages 248–255, 2009.

APPENDIX A. PROOFS

Proof for lemma 1

Both \mathbf{A} and \mathbf{B} can be seen as points in an N -dimensional (N -D) space. Since both of them are unit l^2 -norm matrices, they land on an N -D hypersphere. Figure 5 shows the 2-D projection of the N -D space.

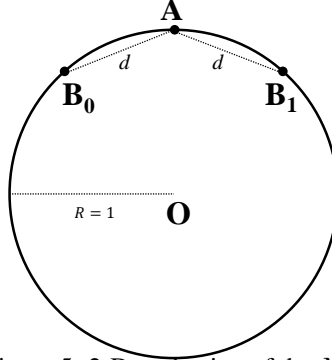


Figure 5: 2-D projection of the N -D space

\mathbf{B}_0 and \mathbf{B}_1 are the border of \mathbf{B} to suffice $|\mathbf{A} - \mathbf{B}|_2 \leq d$. In the N -D space, assume the surface area of $\odot \mathbf{O}$ is $S_{\mathbf{O}}$, surface area of hypersurface $\widehat{\mathbf{B}_0 \mathbf{A} \mathbf{B}_1}$ is $S_{\mathbf{B}_0 \mathbf{A} \mathbf{B}_1}$, then:

$$P_1 = \frac{S_{\mathbf{B}_0 \mathbf{A} \mathbf{B}_1}}{S_{\mathbf{O}}} \quad (18)$$

Now we make an auxiliary sphere $\odot \mathbf{A}$ with $r_{\mathbf{A}} = d$, as shown in figure 6:

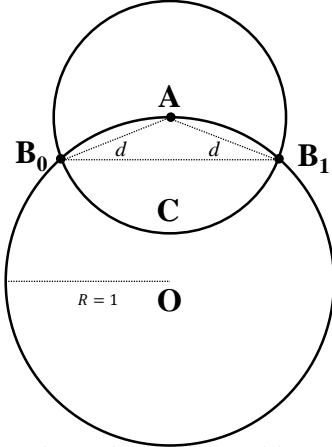


Figure 6: Add the auxiliary sphere

In the 2-D projection, we can see that the length of arc $\widehat{\mathbf{B}_0 \mathbf{A} \mathbf{B}_1}$ is smaller than the length of arc $\widehat{\mathbf{B}_0 \mathbf{C} \mathbf{B}_1}$, as the latter is further away from the straight line $\overline{\mathbf{B}_0 \mathbf{B}_1}$. Similarly, in the N -D space, the area of hypersurface $\widehat{\mathbf{B}_0 \mathbf{A} \mathbf{B}_1}$ is smaller than the area of hypersurface $\widehat{\mathbf{B}_0 \mathbf{C} \mathbf{B}_1}$. Therefore, we have equation 19:

$$P_1 \leq \frac{S_{\mathbf{B}_0 \mathbf{C} \mathbf{B}_1}}{S_{\mathbf{O}}} \leq \frac{\frac{1}{2} S_{\mathbf{A}}}{S_{\mathbf{O}}} \quad (19)$$

where $S_{\mathbf{A}}$ is the surface area of $\odot \mathbf{A}$. The N -D hypersphere surface area formula can be represented as equation 20:

$$S_N(R) = \frac{2\pi^{\frac{N+1}{2}}}{\Gamma(\frac{N+1}{2})} R^{N-1} \quad (20)$$

Substitute equation 20 into equation 19, we can get:

$$P_1 \leq \frac{1}{2} d^{N-1} \quad (21)$$

Therefore, lemma 1 is proven.

Proof for lemma 2

The sum of squared error (SSE) between \mathbf{D}^r and \mathcal{D}^r can be calculated by equation 22:

$$S(\mathbf{D}^r, \mathcal{D}^r) = (\mathbf{D}^r - \mathcal{D}^r)^T \cdot (\mathbf{D}^r - \mathcal{D}^r) \quad (22)$$

Substitute $\mathbf{D}^r = \mathbf{T}^r \cdot \mathbf{M}^{-1}$ and $\mathcal{D}^r = \mathbf{T}^r \cdot \mathbf{G}$ into equation 22 we can get equation 23:

$$\begin{aligned} S(\mathbf{D}^r, \mathcal{D}^r) &= (\mathbf{T}^r \cdot \mathbf{M}^{-1} - \mathbf{T}^r \cdot \mathbf{G})^T \cdot (\mathbf{T}^r \cdot \mathbf{M}^{-1} - \mathbf{T}^r \cdot \mathbf{G}) \\ &= (\mathbf{T}^r \cdot (\mathbf{M}^{-1} - \mathbf{G}))^T \cdot (\mathbf{T}^r \cdot (\mathbf{M}^{-1} - \mathbf{G})) \\ &= \mathbf{T}^{rT} \cdot (\mathbf{M}^{-1} - \mathbf{G})^T \cdot (\mathbf{M}^{-1} - \mathbf{G}) \cdot \mathbf{T}^r \end{aligned} \quad (23)$$

For easy representation, assert $\mathbf{K} = (\mathbf{M}^{-1} - \mathbf{G})^T \cdot (\mathbf{M}^{-1} - \mathbf{G})$. Equation 23 can be simplified to equation 24:

$$S(\mathbf{D}^r, \mathcal{D}^r) = \mathbf{T}^{rT} \cdot (\mathbf{M}^{-1} - \mathbf{G})^T \cdot (\mathbf{M}^{-1} - \mathbf{G}) \cdot \mathbf{T}^r = \mathbf{T}^{rT} \cdot \mathbf{K} \cdot \mathbf{T}^r \quad (24)$$

Since \mathbf{K} is a symmetrical matrix, it can be factorized into the product of unitary matrix and diagonal matrix, as shown in equation 25:

$$\mathbf{K} = \mathbf{P}^T \cdot \mathbf{\Lambda} \cdot \mathbf{P} \quad (25)$$

where \mathbf{P} is an unitary matrix and $\mathbf{\Lambda}$ is a diagonal matrix. Substitute equation 25 into equation 23 we can get equation 26:

$$\begin{aligned} S(\mathbf{D}^r, \mathcal{D}^r) &= \mathbf{T}^{rT} \cdot \mathbf{P}^T \cdot \mathbf{\Lambda} \cdot \mathbf{P} \cdot \mathbf{T}^r \\ &= \sum_{i=0}^{N'-1} \Lambda_{ii} (\mathbf{P} \cdot \mathbf{T}^r)_i^2 \end{aligned} \quad (26)$$

Where N' is the number of elements in \mathbf{T}^r . Since \mathbf{T}^r is the linear transformation of a nature data \mathbf{D}^r , we assume the elements in \mathbf{T}^r is approximately independent and identically distributed, then we can get:

$$\sum_{i=0}^{N'-1} E((\mathbf{P} \cdot \mathbf{T}^r)_i^2) = 1 \quad (27)$$

where E means expectation. Additionally, from equation 26, we can have:

$$E(S(\mathbf{D}^r, \mathcal{D}^r)) = \sum_{i=0}^{N'-1} \Lambda_{ii} E((\mathbf{P} \cdot \mathbf{T}^r)_i^2) \quad (28)$$

Combining equation 27 and 28, we can get:

$$\begin{aligned} \sum_{i=0}^{N'-1} E((\mathbf{P} \cdot \mathbf{T}^r)_i^2) &= 1 \\ \Rightarrow E((\mathbf{P} \cdot \mathbf{T}^r)_i^2) &= \frac{1}{N'} \\ \Rightarrow E(S(\mathbf{D}^r, \mathcal{D}^r)) &= \frac{\sum_{i=0}^{N'-1} \Lambda_{ii}}{N'} = \frac{Tr(\mathbf{\Lambda})}{N'} \end{aligned} \quad (29)$$

where Tr is the trace of matrix, meaning the sum of all diagonal elements. According to equation 25, $Tr(\mathbf{\Lambda}) = Tr(\mathbf{K})$. Therefore we can represent $Tr(\mathbf{\Lambda})$ by \mathbf{G} and \mathbf{M}^{-1} , as shown in equation:

$$Tr(\mathbf{\Lambda}) = Tr(\mathbf{K}) = \sum_{i=0}^{N''-1} (\mathbf{M}^{-1} - \mathbf{G})_i^T \cdot (\mathbf{M}^{-1} - \mathbf{G})_i \quad (30)$$

where $(\mathbf{M}^{-1} - \mathbf{G})_i$ denotes the column vector in $(\mathbf{M}^{-1} - \mathbf{G})$ with the index of i , N'' is the number of columns in $(\mathbf{M}^{-1} - \mathbf{G})$. According to the rules of d2r, $N'' = N'$. Substitute equation 30 into equation 29, we can get:

$$\begin{aligned} E(S(\mathbf{D}^r, \mathcal{D}^r)) &= \frac{1}{N'} \sum_{i=0}^{N'-1} (\mathbf{M}^{-1} - \mathbf{G})_i^T \cdot (\mathbf{M}^{-1} - \mathbf{G})_i \\ &= \frac{1}{N'} \sum_{i=0}^{N'-1} \sum_{j=0}^{N'-1} (\mathbf{M}^{-1} - \mathbf{G})_{i,j}^2 \end{aligned} \quad (31)$$

At this point, we have successfully established the correlation between $S(\mathbf{D}^r, \mathcal{D}^r)$ and $(\mathbf{M}^{-1} - \mathbf{G})$. Additionally, we scale the norm of \mathbf{M}^{-1} and \mathbf{G} to N' , which means:

$$\sum_{i=0}^{N'-1} \sum_{j=0}^{N'-1} (\mathbf{M}_{i,j}^{-1})^2 = \sum_{i=0}^{N'-1} \sum_{j=0}^{N'-1} \mathbf{G}_{i,j}^2 = N' \quad (32)$$

The normalized \mathbf{M}^{-1} and \mathbf{G} can be seen as two points in a hypersphere with the radius of $R = \sqrt{N'}$. The l^2 distance d between \mathbf{M}^{-1} and \mathbf{G} is:

$$d = \sqrt{\sum_{i=0}^{N'-1} \sum_{j=0}^{N'-1} (\mathbf{M}_{norm}^{-1} - \mathbf{G}_{norm})_{i,j}^2} \quad (33)$$

Combining equation 31 and equation 33, we can get:

$$d = \sqrt{E(S(\mathbf{D}^r, \mathcal{D}^r))N'} \quad (34)$$

According to the correlation between SSE and MPE, $E(S(\mathbf{D}^r, \mathcal{D}^r)) = E_{sd}^2(\mathbf{D}^r, \mathcal{D}^r) \leq \sigma^2$, therefore:

$$d \leq \sigma \sqrt{N'} \quad (35)$$

Re-scale the space by the factor of $\frac{1}{\sqrt{N'}}$, we can get $d \leq \sigma$ and $R = 1$.

Additionally, the dimension of the space N equals to the total number of elements in \mathbf{M}^{-1} . Therefore $P_2 = P_1(d = \sigma)$ and lemma 2 is proven.

APPENDIX B. ADDITIONAL FIGURES



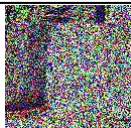


Privacy Reservation	Original	$\sigma = 5\text{E-}5$	$\sigma = 5\text{E-}4$	$\sigma = 5\text{E-}3$	0.5
Cat photo					

Figure 7: Cat photos with different privacy reservation limits.